Biogeosciences, 17, 3545–3561, 2020
https://doi.org/10.5194/bg-17-3545-2020

Biogeosciences Open Access EGU

Better molecular preservation of organic matter in an oxic than in a sulfidic depositional environment: evidence from *Thalassiphora pelagica* (Dinoflagellata, Eocene) cysts

Gerard J. M. Versteegh[1,2], **Alexander J. P. Houben**[3,4], **and Karin A. F. Zonneveld**[2]

[1]Heisenberg Group Marine Kerogen, Marum Research Faculty, Universität Bremen, 28359 Bremen, Germany
[2]Micropaleontology Group, Division Marine Palynology, Marum Research Faculty,
Universität Bremen, 28359 Bremen, Germany
[3]Geological Survey of the Netherlands, TNO, 3548 CB Utrecht, the Netherlands
[4]Marine Palynology and Palaeoceanograhy, Faculty of Geosciences, Utrecht University, Budapestlaan 4,
3584 CD Utrecht, the Netherlands

Correspondence: Gerard J. M. Versteegh (versteeg@uni-bremen.de)

Received: 16 September 2019 – Discussion started: 28 October 2019
Revised: 12 May 2020 – Accepted: 4 June 2020 – Published: 9 July 2020

Abstract. Anoxic sediments, as compared to oxic settings, encompass a much higher proportion of relatively labile and thus more reactive organic matter, naturally giving rise to structural changes of the organic molecules themselves, as well as cross-linking between them (e.g., through reactive sulfur species). Both processes transform the original biomolecules into geomolecules. For the oxic environment, these intermolecular and intramolecular transformations also operate, but cross-linking may be less important since the labile, reactive component is rapidly removed. As such, one may expect a structurally better preservation of the more refractory initial biomolecules in the oxic environment. To test this hypothesis, initially identical biomolecules need to be compared between different preservational environments. Here, we use the species-specific morphology of organic microfossils to assure a single initial biosynthetic product (the cysts of the fossil dinoflagellate species *Thalassiphora pelagica*) for comparison. We assess the macromolecular structures of cysts from the Eocene (~ 40 Ma) sulfidic Rhine Graben and the oxic Kerguelen Plateau and compare them with each other and the structures of recent cysts. While between the sites the *T. pelagica* cysts are morphologically identical and show no signs of morphological modification, pyrolysis gas chromatography mass spectroscopy and micro Fourier transform infrared analyses show that their macromolecular characteristics are strongly different. Comparison with recent cysts shows that the cysts deposited in the sulfidic Rhine Graben show a strong additional contribution of long-chain aliphatic moieties and thus less diagenetic intermolecular cross-linking. The presence of organic sulfur identifies natural volcanization as one of the diagenetic processes. Furthermore, we observe a loss of bound oxygen and no trace of the original carbohydrate signature of the cyst wall biomacromolecule. The material deposited in the oxic sediments of the Kerguelen Plateau shows no traces of sulfurization. It shows a minor contribution of short carbon chains only and thus less diagenetic intermolecular cross-linking. Furthermore, a carbohydrate signature was still preserved evidencing a better molecular preservation of the initial biomacromolecule, supporting our initial hypothesis. This shows that excellent morphological preservation does not imply excellent chemical preservation. It also leads to the conclusion that the best preservation of molecular structure is not necessarily where most organic matter gets preserved, which, in turn, is important for understanding the nature and fate of sedimentary organic matter and its isotopic signature.

Published by Copernicus Publications on behalf of the European Geosciences Union.

1 Introduction

Kerogen, the insoluble sedimentary organic matter (OM) is by far the largest OM pool on Earth (Durand, 1980). It plays an important role in the biogeochemical cycles of carbon and related elements, fossil fuel formation, and is a source of information on the history of life and environments. Despite considerable advances in elucidating the nature of kerogen over the last few decades, many aspects of its formation, modification and structure at a molecular level are still far from understood (de Leeuw and Largeau, 1993; Vandenbroucke and Largeau, 2007; Schiffbauer et al., 2014). This is particularly true for marine kerogen, where the heterogeneity and the small size of the kerogen particles are complicating factors in the effort to understand kerogen formation and modification.

Organic microfossils are a special kind of kerogen, since for many of them their specific morphology provides a direct link between the biological source, the initial biomacromolecule (often at species level) and the modified fossil geomacromolecule for different environments and time slices. As such an analysis of their molecular structure has the great advantage of knowing the initial molecular structure, we can separate the contributions of biosynthesis and postmortem modification on the final kerogen structure.

The preservation of OM at molecular level and visible level, i.e., its apparent morphology, may be very different.

Chemical analysis of organic (micro)fossils has shown that, despite excellent morphological preservation, molecular preservation may be poor, even to the extent that no recognizable trace of the original biomolecules is preserved (e.g., Stankiewicz et al., 1998, 2000; de Leeuw et al., 2006; Gupta et al., 2007).

At a molecular level, we consider the accumulating diagenetic structural difference between the resulting geomolecule and the initial biomolecule as an accumulating reduction of the molecular preservation. In practice, the degree of molecular preservation will be the extent to which the initial biomolecule can still be recognized by means of various analytical methods. The molecular changes may be diagenetic cross-linking (kerogenization, sensu Butterfield, 1990) but include also other kinds of structural changes, such as modifying bonds and functional groups or changing stereochemistry. These changes may take place aerobically or anaerobically and may be intramolecular (changing itself) or intermolecular (between molecules). The latter case may cause other molecules to become structural elements of the resulting geomolecule. Since this addition of structural elements can involve many different types of molecules, we prefer to use intermolecular cross-linking rather than polymerization, which assumes a limited set of similar monomers. In oxic settings, OM degradation is mostly severe and highly selective, but nevertheless processes like photodegradation and intermolecular and intramolecular oxidative cross-linking may lead to condensation of the OM early in the fossilization process, which reduces OM degradability, creates macromolecules from lipids and transforms biomacromolecules into geomacromolecules (e.g., Harvey et al., 1983; Gatellier et al., 1993; Versteegh et al., 2004; Rontani, 2008). In anoxic settings OM degradation is much less complete, often leading to the formation of organic-rich sediments (e.g., Bianchi et al., 2016). Here, condensation of OM may occur in various ways, catalyzed by clay minerals or reduced metal ions and brought about by reactive sulfur species. Of these processes the natural sulfurization has received ample attention, and this process seems especially effective in the absence of reactive Fe, which has the potential to outcompete organic molecules for reactive polysulfides and limit OM sulfurization (Nissenbaum and Kaplan, 1972; Kohnen et al., 1989; Kutuzov et al., 2019).

In comparison to anaerobic postmortem modification of sedimentary OM, little attention has been paid to the signature of aerobic processes in the geomacromolecular structure, despite the importance of aerobic modification of OM since the Great Oxidation Event.

Most of these insights have been obtained by analyzing different taxa from unique sedimentary environments, which makes it hard to obtain insight into the relation between the species-specific properties of its organic product and the subsequent postmortem modification. To better separate the initial OM and postmortem modification, ideally one would analyze the same biomacromolecule from different environmental settings.

Here we elucidate the influence of differing sedimentary environments on the chemical preservation of same species, i.e., fossil dinoflagellate cysts of *Thalassiphora pelagica*.

By far the majority of the cysts producing dinoflagellates are either peridinioid or gonyaulacoid. The peridinioids are generally heterotrophic and produce brown cysts, whereas the gonyaulacoids (such as cysts of *T. pelagica*) are mostly phototrophic and produce colorless cysts. Cyst degradation experiments using moorings in surface sediments and near oxidation fronts have demonstrated that the brown peridinioid cysts rapidly degrade in oxic environments; notably, *Echinidinium* spp. and *E. aculeatum* also degrade in suboxic environments. In contrast to this, the transparent gonyaulacoid cysts are much more resistant and often survive millennia of oxic conditions (Zonneveld et al., 2010, 2019 and references therein). These differences in degradability are also reflected in the different molecular structures of the walls of organic dinoflagellate cysts, which vary considerably between species (e.g., Bogus et al., 2014; Mertens et al., 2016; Gurdebeke et al., 2018). They all seem to consist of a carbohydrate backbone with various contributions of proteinaceous material that appears to be species-specific (Versteegh et al., 2012; Bogus et al., 2014). Basically the same variability has been reported from fossil material where the molecular structure could even be used to distinguish between closely related *Apectodinium* species (Bogus et al., 2012). However, it became apparent that in some cases postmortem

modification may considerably change the molecular structure of the cyst wall. For instance, contributions of long-chain aliphatic moieties have been reported for *Chiropteridium* spp. (de Leeuw et al., 2006) and *T. pelagica* cysts from the Oligocene Rhine Graben (Versteegh et al., 2007). These modifications may be so pronounced that the original signature is largely lost (de Leeuw et al., 2006; Versteegh et al., 2007). However, the extent to which environment transforms the initial biomacromolecule to its geomacromolecular derivate is still to a large extent terra incognita.

Here we concentrate on the impact of oxic versus anoxic sedimentary environments on the macromolecular structure of *T. pelagica* cysts. *T. pelagica* belongs to the transparent gonyaulacoid dinoflagellates and thus belongs to the group of cysts resistant to aerobic degradation. This resistance enables our comparison in the first place. Characterization of the molecular composition of the cyst walls with Fourier transform infrared (FTIR) micro-spectroscopy, pyrolysis gas chromatography mass-spectrometry (py-GC-MS) and thermally assisted hydrolysis and methylation (THM)-GC-MS showed that the cyst wall macromolecule of these cysts is relatively condensed, which is in line with the condensation of an initially carbohydrate-based wall biomacromolecule. Nevertheless, an average chain length of ~ 12 carbon atoms was recorded, which was explained by postmortem addition of carboxylic acids by early sulfurization of the cysts in the anoxic to suboxic setting of the depositional environment. These carboxylic acids were most probably polyunsaturated and derived from the membranes and lipid bodies of the once living cell inside the cyst. The sulfur species readily attack functionalized groups, such as double bonds, ketones and aldehydes in OM (Viaravamurthy and Mopper, 1987; Schouten et al., 1994a, b; Hebting et al., 2006) and are thus well suited to cross-link unsaturated fatty acids and other functionalized components to the carbohydrate-based cyst wall macromolecule. Here we compare the results of the study on anoxically deposited and sulfurized *T. pelagica* cysts to new analysis of cysts of the same species that have been deposited in an oxic depositional environment. This allows us to determine the diagenetic effects of aerobic versus anaerobic sulfate-reducing environments on the molecular structure of organic microfossils.

2 Material and methods

The *T. pelagica* cysts from the oxic depositional environment (Kerguelen Plateau) have been collected during IODP Leg 120 Site 748B (58°26.45′ S, 78°58.89′ E) and have been isolated from sample 18H 17W 55–57 cm. The sample is derived from 152.6 m below the seafloor from the upper part of unit II, consisting of nannofossil ooze with an organic carbon content < 0.2 % and a sedimentation rate of about 0.6 cm ka^{-1}. This typically open oceanic environment must have been well ventilated at the seafloor, and considering the low sedimentation rate and low OM content, the sediment has clearly been subject to long and extensive aerobic degradation prior to reaching a burial depth below the oxic–suboxic interface. The sample was deposited during the Middle Eocene Climatic Optimum, at about 40 Ma (Schlich et al., 1989). The sample was crushed and minerals were removed using HCl (36 %) and HF (40 %) at room temperature. The sample was washed, and the > 20 µm fraction was mounted to enable palynofacies analysis by light microscope.

The material from the Rhine Graben from the Middle Rupelian (Oligocene) has an age of about 31 Ma. At that time the Rhine Graben was a restricted and narrow basin connecting the Tethys Ocean with the North Sea. The material has been deposited in a sulfate-reducing environment. The sample is derived from the Fischschiefer Unit, consisting of 80 m of bituminous, finely laminated marly clay and silt stones typically with an organic carbon content > 3 % and deposited about 1.8 Ma, representing an average sedimentation rate of 4.4 cm ka^{-1}. The environment experienced anoxia in the water column and sediment (Pross, 2001). Freshly formed cysts sinking to the seafloor as such experienced only minimal aerobic degradation (Pross and Schmiedl, 2002). The sample was carefully cleaned and about 50 g of sediment was crushed and treated with 20 % HCl to remove carbonates. Subsequently, the sample was repeatedly treated ultrasonically and washed over a 125 µm sieve. The cysts were picked for FTIR micro-spectroscopy and for py-GC-MS and THM-GC-MS from the 315–125 µm fraction. HF or oxidizing agents such as HNO_3 or H_2O_2 have not been used.

2.1 FTIR analysis

Preliminary analyses using transmission, reflection and attenuated total reflection (ATR) spectroscopy showed that, for our material, ATR analyses provided the best results with respect to S/N ratio and scattering. Furthermore, to reduce the effects of instrument- and measurement-method-dependent differences between the spectra of the taxa compared, we remeasured cysts of *T. pelagica* (Versteegh et al., 2007) from the Rhine Graben and the culture-derived cysts of *Lingulodinium polyedrum* (Versteegh et al., 2012) using the same instrument and protocol. At least three cysts were analyzed twice for each sample by micro-FTIR after cleaning the cysts with distilled water and methanol. Only specimens that were visually clean were measured. Measurements were made with a BRUKER Invenio-S spectrometer coupled to a Hyperion 1000 IR microscope equipped with a KBr beam splitter and liquid N_2-cooled mercury cadmium telluride (MCT) detector. A total of 256 scans were obtained at 4 cm^{-1} resolution using a germanium ATR crystal of 100 µm diameter. The spectra were corrected for atmospheric CO_2 and baseline corrected using a concave rubber band correction with 64 baseline points and 5 iterations. The ATR spectra have been transformed such that the position and intensity of the absorption bands are similar to transmission spectra by using

the advanced ATR correction algorithm with an average refraction index of 1.5, a 45° angle of incidence and one ATR reflection as parameters (Nunn and Nishikida, 2008). Assignments of characteristic IR group frequencies follow Colthup, Daly and Wiberly (1990) and published literature. For calculation of the first and second derivatives and fitting of Gaussian curves using the Levenberg–Marquardt algorithm, the software package Fytik 1.2.1 has been used (Wojdyr, 2010).

2.2 Pyrolysis and thermally assisted hydrolysis and methylation gas chromatography–mass spectrometry

The cysts from the Kerguelen Plateau were solvent extracted and transferred to a quartz tube (CDS 10A1-3015) for pyrolysis. For thermally assisted hydrolysis and methylation (THM) in the presence of tetramethylammonium hydroxide (TMAH) about 0.2 mL of 10 % aqueous TMAH was added and the quartz tube was oven dried for 1 h at 60 °C. The sample was inserted in a CDS 5200 pyrolysis unit and kept for 5 min at 700 °C. The pyrolysate and thermochemolysate were transferred to a gas chromatograph Agilent 7890A series using a 300 °C interface and transfer line temperature. Sample injection was in splitless mode with a delay time of 6 min. An HP5MS GC column was used of 30 m length, 0.25 mm diameter and 0.25 µm film thickness. The GC conditions were 3 min isotherm at 40 °C, followed by a temperature increase of 15 °C min^{-1} up to 130 °C, an increase of 8 °C min^{-1} to 250 °C and finally an increase of 20,°C min^{-1} to 320 °C. The final temperature was held for 5 min. The interface between GC and MS was at 280 °C. For mass spectrometry, an Agilent 5975C MSD was used in full scan mode (mass range m/z 50–500 with 3.25 scans s^{-1} at 70 eV). Compound identification was performed using the NIST spectral library and relative retention times. Relative retention times were calibrated in comparison with a mixture of *n*-alkane standards run prior to each analysis.

For pyrolysis and thermochemolysis gas chromatography–mass spectrometry of the cysts from the Rhine Graben (see also Versteegh et al., 2007), the purified cysts were transferred to a quartz tube (CDS 10A1-3015) for pyrolysis. For thermochemolysis in the presence of TMAH about 0.2 mL of 10 % aqueous TMAH was added, and the quartz tube was oven dried for 1 h at 60 °C. The sample was inserted in a CDS AS2500-plus pyrolysis unit and kept for 5 min at 700 °C. The pyrolysate and thermochemolysate were transferred to an Agilent 6090N series gas chromatograph using a 280 °C interface temperature in splitless mode with a 6 min delay time. The GC column HP5MS was of 30 m length, 0.25 mm diameter and 0.25 µm film thickness. The GC conditions were a 3 min isotherm at 40 °C, 15 °C min^{-1} to 130 °C, 8 °C min^{-1} to 250 °C, 20 °C min^{-1} to 320 °C and 5 min isotherm. The interface temperature was 280 °C GC to MS. For mass spectrometry an Agilent 5973 MSD was used in full scan mode (mass range m/z 50–500, 3.25 scans s^{-1}, 70 eV). Prior to each analysis a mixture of *n*-alkane standards was analyzed to check for contaminants and calibrate retention times.

Compound identification was performed using the NIST spectral library and relative retention times. Furthermore, we used our internal library that is based upon decades of collection of spectra with relative retention times of a wide variety of standards and natural and pyrolysis products.

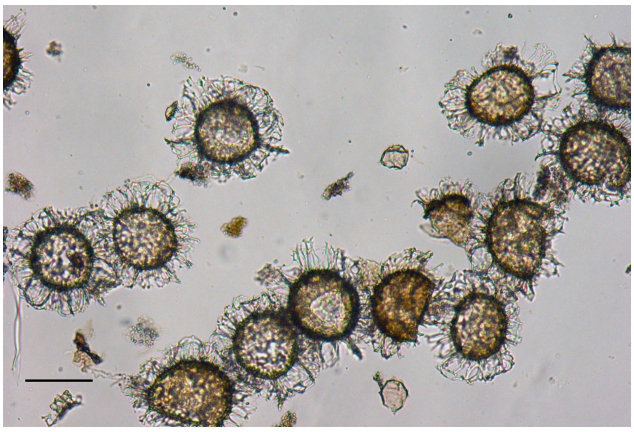

Figure 1. Microphotograph of the *Thalassiphora pelagica* assemblage from the Kerguelen Plateau prior to purification with a sieve with 50 µm pore size. Scale bar = 100 µm.

3 Results

3.1 Palynofacies analysis

The assemblage consists of a nearly mono-typical assemblage *T. pelagica* cysts with occasional *Phthanoperidinium* and indeterminable organic debris (Fig. 1). The residue left after additional purification with a sieve with 50 µm pore size consisted of *T. pelagica* cysts only.

3.2 FTIR micro-spectroscopy

The FTIR spectra are very similar for the specimens from the same sample, but there are consistent differences between the spectra of specimens from the different samples. Therefore, only the average spectrum is shown for each sample (Fig. 2). The spectra can be divided into six absorption bands (A–F). The second derivative reveals the locations of absorption maxima and shoulders in much more detail (Fig. 3).

3.2.1 The FTIR spectra of the *T. pelagica* cysts from the oxidized depositional environment (Kerguelen Plateau)

The absorption of band A (3700–3000 cm^{-1}), centered at 3400 cm^{-1}, is assigned to alcoholic OH, phenolic OH and/or carboxylic OH.

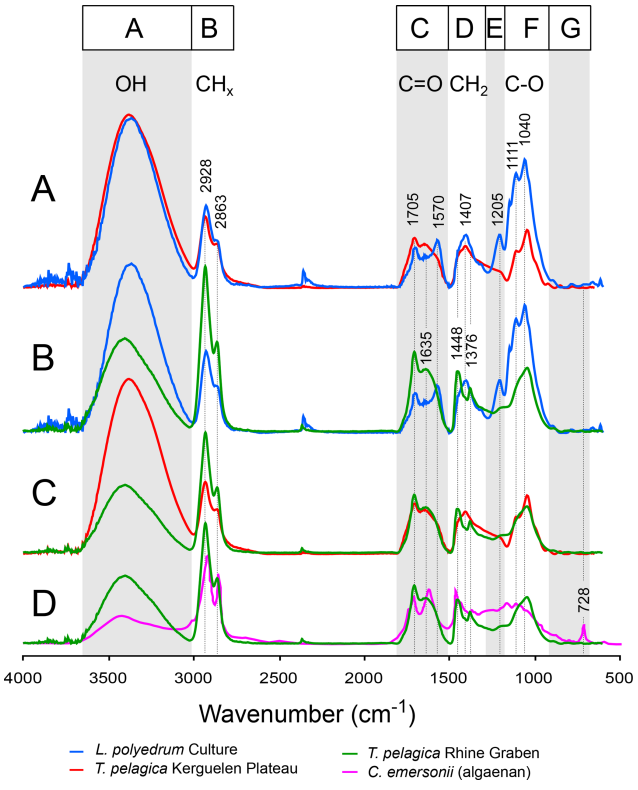

Figure 2. Pairs of micro-Fourier transform infrared ATR spectra of algae: *Lingulodinium polyedrum* cysts from culture (blue line), a remeasured sample of Versteegh et al. (2007); *Thalassiphora pelagica* cysts from the Kerguelen Plateau (red line); *Thalassiphora pelagica* from the Rhine Graben (green line), a remeasured sample of Versteegh et al. (2007); and *Chlorella emersonii* (pink line) (adapted from Allard and Templier, 2000). For further explanation see the text.

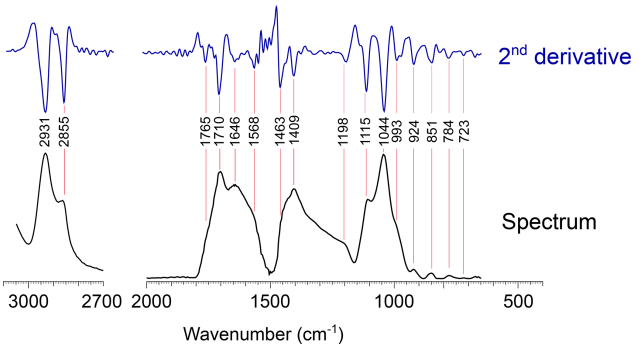

Figure 3. Detailed views of the FTIR spectrum of *Thalassiphora pelagica* from the Kerguelen Plateau with the second derivative. **(a)** Detail of the 3500–2500 cm^{-1} region of the FTIR absorption spectrum (transmission mode) of *T. pelagica*. **(b)** Detail of the 2000–700 cm^{-1} region with the maxima of the spectrum second derivative showing the locations of absorption bands.

The strong, narrow aliphatic absorptions of band B (3000–2700 cm^{-1}), centered at 2928 and 2863 cm^{-1}, are assigned to antisymmetric stretching vibrations from CH_2 and symmetric stretching vibrations from CH_2 methylene groups, respectively. Further deconvolution shows that a third Gaussian–Lorentzian band at 2892 cm^{-1} is required to model this part of the spectrum (Fig. 4). This third band is attributed to CH stretch. There is a marked absence of evidence for absorptions by CH_3. In algal walls such a low contribution of methyl groups is typically associated with the presence of long aliphatic chains in the wall macromolecule, such as the algaenan of, e.g., *Chlorella emersonii* (Fig. 2). However, the corresponding absorption of CH_2 in long carbon chains near 723 cm^{-1} (see also McMurry and Thornton, 1952) is also absent from our spectra, leading to the conclusion that the *T. pelagica* wall macromolecule consists primarily of short carbon chains without free methyl groups, which is in agreement with the pyrolysis- and spectroscopy-based hypothesis that the gonyaulacoid dinoflagellate cyst walls (such as, e.g., *L. polyedrum*) primarily consist of a carbohydrate-based biopolymer (Versteegh et al., 2012).

For band C (1800–1500 cm^{-1}) we assign the absorption centered at 1705 cm^{-1} and the shoulder at 1768 cm^{-1} to the vibration of carbonyl C = O. Hereby, the absorption at 1705 cm^{-1} may represent α and β unsaturated aliphatic ketones or hydrogen bonding in carboxylic acid dimers (Colthup et al., 1990); the corresponding enol tautomers may provide a second explanation for the moderate absorption centered at 1612 cm^{-1}.

For band D (1500—1300 cm^{-1}), the absorption at 1411 cm^{-1} may be attributed to deformation of CH_2 next to carbonyls. Alternatively, the absorption at 1411 cm^{-1} may arise from olefin CH rocking. We relate absorptions at 1463 cm^{-1} to a scissor deformation of CH_2. There is no clear symmetric umbrella deformation of C-CH_3 at 1375 cm^{-1} of hydrocarbons, which agrees with the absence of evidence for methyl groups in band B.

For bands E to G, the weakly defined absorptions between 1305 and 1203 cm^{-1} (band E; 1300–1150 cm^{-1}) can be related to C-O carboxylic acids. The absorptions in band F (1150–900 cm^{-1}) at 1112, 1047 and 986 cm^{-1} are assigned to C-O, e.g., as C-O-C and C-O-H of carbohydrates. For band G, the minor absorption at 728 cm^{-1} is attributable to CH_2 rock and its low intensity agrees with only a minor contribution of predominantly short carbon chain < 4 CH_2 sequences (McMurry and Thornton, 1952).

As such the spectrum indicates a relatively short-chain polymer. The absence of evidence for CH_3 indicates it to be heavily branched and/or functionalized. The richness in C-O and O-H suggests the functionalities to be primarily hydroxyl groups and ether bonds with a much lower abundance of carbonyl groups, a combination typically found in carbohydrate-based polymers. There is no evidence for an aromatic contribution, but some aliphatic C = C can not be excluded.

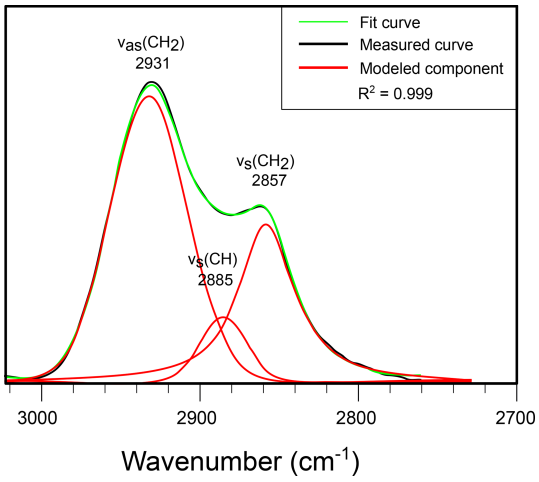

Figure 4. Deconvolution of the CH_x absorption bands for the 3100–2700 cm^{-1} region demonstrating the absence of significant CH_3 absorption. Modeled curves are Lorentzian (curve at 2931 cm^{-1}) and Gaussian (the other curves).

3.2.2 The FTIR spectra of reanalyzed cultured *L. polyedrum* cysts and *T. pelagica* cysts from the Rhine Graben

The new spectra for *L. polyedrum* differ from the published spectrum (Versteegh et al., 2012): we measured in ATR mode, and the published spectrum was obtained in reflection mode. After also remeasuring in reflection mode, our spectrum was very similar to the published one (Supplement Fig. S1), confirming that the observed differences result from the different mode of measurement and spectrum correction. The much larger relative abundance of bands A and B and reduction of band F result from a wavenumber-dependent amplification of the absorption of the ATR correction algorithm. As such the differences between the published spectra and those presented here predominantly result from different measurement and spectrum correction algorithms and do not require a new spectral interpretation. Since Mie scattering causing spectrum distortion plays a relatively large role for these small objects in reflection mode (Herman, 1962), we use the corrected ATR spectra for comparison.

The new ATR spectra obtained for *T. pelagica* from the Rhine basin are closely similar to the transmission spectrum published, except for band F (Fig. S2), which was much weaker in the spectra of Versteegh et al. (2007). This difference is unlikely to be accounted for by degradation of the sample since over the years it has been kept frozen at −20 °C in distilled water. Here we also attribute the observed difference to the different modes of measurement (ATR versus transmission) and the difficulty of measuring single cysts in transmission mode. The interpretation of the absorption bands is similar to that for the specimens from the Kerguelen plateau, but there are large differences in relative strengths of these bands, notably the stronger relative absorptions of B, C and (to some extent) D.

3.3 Pyrolysis–GC-MS

The pyrolysate (Fig. 5; Table 1) contains both aliphatic and aromatic moieties. There is a considerable amount of oxygen containing saturated and unsaturated non-aromatic moieties with 5-membered and 6-membered rings and up to three additional carbon atoms amongst which are furans, cyclopentenones, cyclopentanones, phenols, benzofurans, indanones and naphthalenones and naphthalenols. Furthermore, there are several series of aromatic moieties. Phenol (m/z 94) and methylated phenols (m/z $94 + 14 \times n$) have been detected up to $n = 4$. Benzene (m/z 78) and alkyl benzenes (m/z $78 + 14 \times n$) have been detected up to $n = 9$. Compounds with more than three carbon atoms attached to naphthalene and indene were not detected. Linear carbon chains play only a minor role and their distribution only becomes apparent from mass chromatograms of their characteristic ions. *n*-Alkenes and *n*-alkanes (m/z 83 and 85) show alkane–alkene pairs for C_7-C_9 and a series of only *n*-alkanes for C_{14}–C_{21}. The mass chromatogram m/z 58 reveals a series of *n*-alkan-2-one–*n*-alken-2-one pairs from C_6-C_{12} and m/z 60 shows C_3-C_{10} alkanoic acids.

The mass distribution in the first 28 min of the chromatogram (Fig. 6) shows that the masses representing aromatic moieties (such as m/z 91, 105, 115, 117, 119, 128 and 129) clearly emerge above their neighbor masses (m/z ±5). The masses representing saturated aliphatic moieties (m/z 57, 71, 85) do not emerge above background as is the case for alkenes > C_5 (m/z 83, 97).

3.4 THM–GC-MS

THM-GC-MS (Fig. 7; Table 2) clearly shows methyl esters of C_3-C_9 and C_{14}–C_{16} *n*-alkanoic acids (C_{17} and C_{18} could not be detected) and C_4-C_9 α, ω dicarboxylic-dimethylesters the latter with a strong preference for the butanedioic moiety. Few oxygen containing aromatic compounds are present. The most prominent are mono- to tri-methoxy benzenes and mono- and dimethoxy benzoic-acid methylesters. Traces of alkane–alkene doublets (using m/z 83/85) are absent.

4 Discussion

4.1 Paleoenvironment

The Rhine Graben restricted marine sedimentary environment is very different from that of the open-ocean Kerguelen Plateau. The Rhine Graben sediments (Pross, 2001) are about 10 Ma younger, and the apparent sedimentation rate (4.4 cm ka^{-1}) and total organic carbon contents (> 3 %) are at least an order of magnitude higher than at the Kerguelen Plateau (sedimentation rate 0.6 cm ka^{-1}; and TOC < 0.2 %,

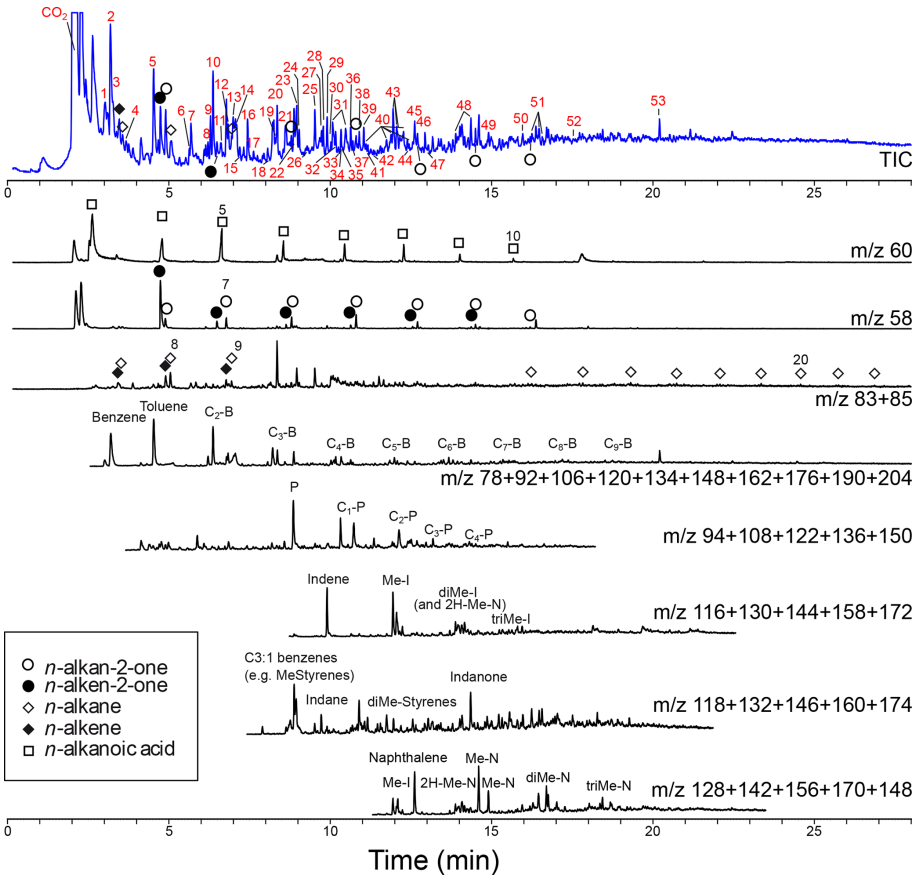

Figure 5. Chromatogram and mass chromatograms of pyrolyzed *Thalassiphora pelagica* cysts from the Kerguelen Plateau. For the total ion current (TIC) the compound names corresponding to numbered peaks (red numbers) are given in Table 1. For the mass chromatograms: B is benzene, P is phenol, N is naphthalene, I is indene, and "C with number" indicates the number of carbon atoms added to the basic structure.

Schlich et al., 1989). However, the most important factor for OM diagenesis and preservation is the redox environment, notably the oxygen exposure time of the OM. With the change from an aerobic redox environment via progressively less powerful electron acceptors to sulfidic conditions, the amount of energy gained during the oxidation of OM also progressively decreases, and OM degradation becomes increasingly thermodynamically limited (Arndt et al., 2013). Therefore, in settings with short oxygen exposure not only the TOC contents but also the concentration of more labile and reactive OM remains much higher over geological time in comparison to equivalent settings with longer oxygen exposure (e.g., Hedges and Keil, 1995; Hoefs et al., 2002; Versteegh et al., 2010; Nierop et al., 2017). Thus, the Rhine Graben sediments with anoxia already in the water column and sulfidic conditions in the sediment never experienced prolonged aerobic degradation. As such, sedimentary organic carbon concentrations are higher, as is the reactivity of this OM in the presence of reactive sulfur species. The Kerguelen sediments experienced much longer oxygen exposure. This exposure was long enough to enable demineralization of most of the OM reaching the seafloor, resulting in sediments lean in OM and where this OM is also refractory. With sedimentation continuing, the sediments containing the *T. pelagica* cysts will have become suboxic over time. However, the refractory nature of the OM and its low concentration severely limit anaerobic intermolecular cross-linking, due to a lack of available substrate. Furthermore, OM mineralization rates will have remained so low that the system never reached sulfate reduction and release of reactive sulfur species. This implies the OM surviving until the environment becomes suboxic may be expected to remain diagenetically relatively unaltered from that moment.

4.2 Comparison of the FTIR spectra (Fig. 2)

Infrared analysis of cysts from surface sediments and dinoflagellate cultures shows that the cysts cluster in two groups (Ellegaard et al., 2013; Bogus et al., 2014): (1) transparent cysts with a cellulose-like cyst wall, such as *Lingulodinium polyedrum* (Versteegh et al., 2012), and (2) brown cysts with a chitin-like cyst wall, such as *Polykrikos kofoidii* (Bogus et al., 2014). The former resist aerobic degradation, the latter aerobically degrade readily. The extinct genus *Tha-*

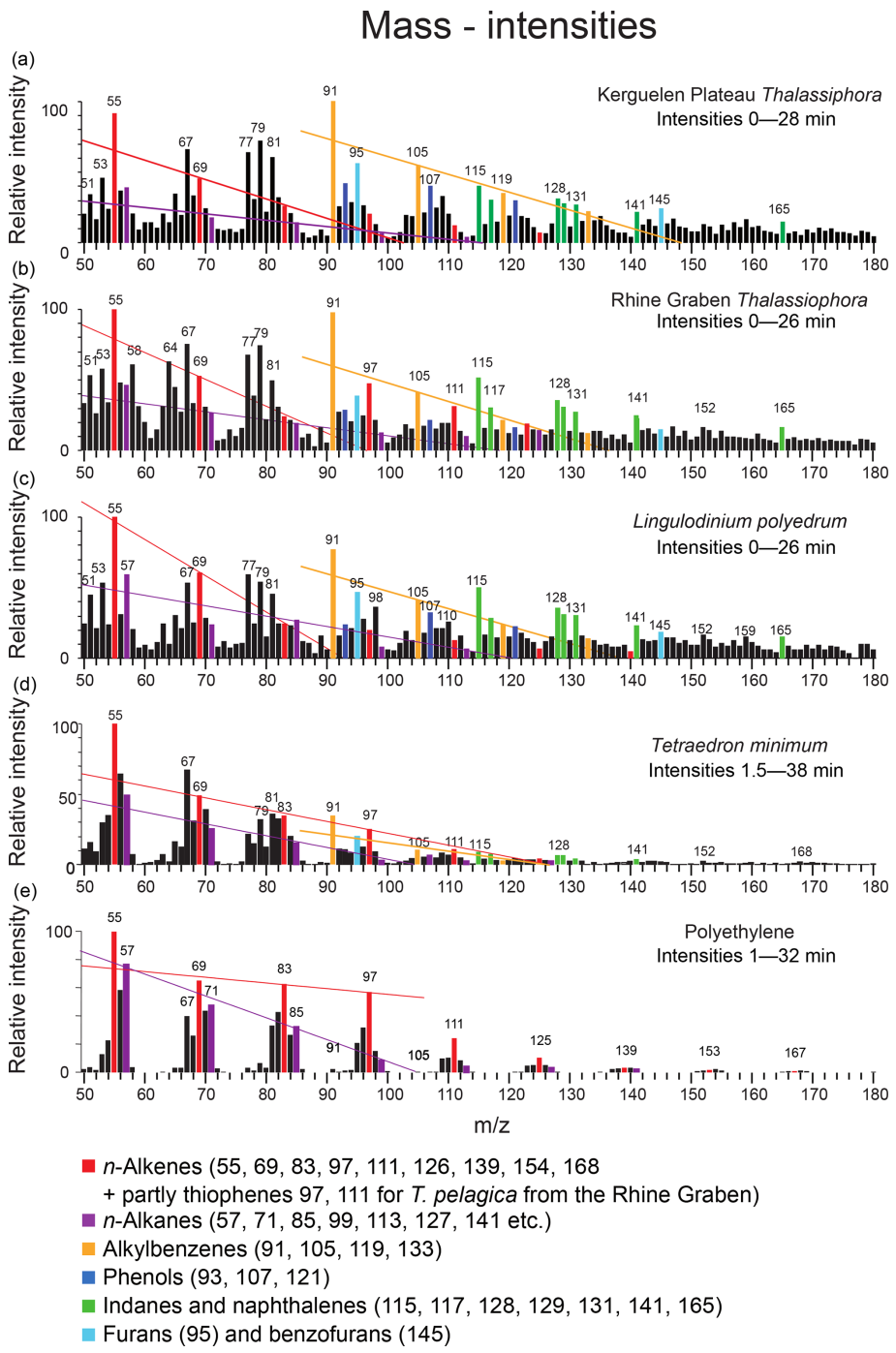

Figure 6. Mass intensity plots of the total chromatograms of **(a)** *Thalassiphora pelagica* from the Kerguelen Plateau, **(b)** *Thalassiphora pelagica* from the Rhine Graben (Versteegh et al., 2007), **(c)** recent *Lingulodinium polyedrum* (Versteegh et al., 2012), **(d)** *Tetraedron minimum* and **(e)** polyethene. The lines connect masses indicative for *n*-alkenes (m/z 69, 83, 97), *n*-alkanes (m/z 57, 71, 85, 99) and alkylbenzenes (m/z 105, 119), respectively. Note that the total ion current of polyethene is dominated by series of ions meeting the criteria C_nH_{2n-1} and C_nH_{2n+1}, reflecting the highly aliphatic nature of the macromolecule. Note the relatively high aromatic contribution for *T. pelagica* (orange bars; m/z 91, 105, 115, 117, 128, 129, 131) in comparison to the "aliphatic-derived" fragments of alkanes and alkenes and the high relative contribution of m/z 97 and 111 for *T. pelagica* from the Rhine Graben as compared to m/z 69 and 83, which is attributed to the presence of alkylthiophenes.

Table 1. Compounds identified in the pyrolysate*.

No.	Name	M+
1	Methylcyclopentadiene (C_6H_8)	80
2	Benzene	78
3	Cyclohexadiene	80
4	2,5-Dimethylfuran	96
5	Toluene	92
6	C_8H_{12}	108
7	Cyclopentenone + Furfural	96 + 82
8	Ethyl-benzene	106
9	2-Propylfuran	110
10	1,3- + 1,4-Dimethylbenzene	106
11	Pentanoic acid	102
12	1,2-Dimethylbenzene	106
13	Styrene	104
14	2-Methyl-2-cyclopentenone (67, 96)	67, 96
15	Acetylfuran	95, 110
16	Cyclopentandione	69, 98
17	Cyclohexenone	68, 96
18	Propylbenzene	120
19	3-Methyl-2-cyclopentenone	96
20	3-Methylbenzene + Unknown (43/85)	120
21	Phenol	94
22	$C_{3:1}$ Benzene + 3-Methylbenzene	118 + 120
23	Cyclohexandione (70,112)	70, 112
24	Octanal	128
25	Methylcyclopentandione (69,112)	112
26	Limonene	136
27	Indane	118
28	2,3-Methylcyclopentenone (67,110)	110
29	Indene	116
30	Methyl-propylbenzene	134
31	Methylphenol	108
32	C_4 Benzene	134
33	C_3 Cyclopentenone (109,124)	124
34	Acetophenone	120
35	Methylbenzaldehyde	120
36	Methylbenzaldehyde	120
37	$C_{3:1}$ Benzene + C_3 Benzene	132 + 134
38	4-Ethenyl-benzene	132
39	Nonenol (no 114)	142
40	C_2 Phenol	122
41	1-Acetylcyclohexene + C_1-Benzofuran	124 + 132
42	3-Ethyl-2-hydroxy-2-cyclopentenone	126
43	Methylindene	130
44	C_5 Benzene	146
45	Naphthalene	128
46	Trimethylphenol (121, 136)	136
47	C_2 Benzofuran	146
48	Indanone + C_2 Indene	132 + 144
49	Methylnaphthalene	142
50	Naphthalenone	146
51	Methylindanone	146
52	C_2 Indanone	160
53	1,3-Diphenylpropane	196

* Peak numbers refer to Fig. 5. C_1 to C_5 (e.g. C_4 Benzene) indicate the number of carbon atoms attached.

Table 2. Compounds identified in the thermochemolysate*.

No.	Name	M+
1	Trimethylamine – TMAH product	59
2	Cyclopentadiene	66
3	$C_{3:1}$ Fatty acid methyl ester	86
4	Cyclohexadiene	80
5	Benzene	78
6	Methyl-cyclohexadiene	94
7	Dimethylamino-acetonitrile – TMAH product	84
8	Toluene	92
9	Ethylbenzene	106
10	1,3- + 1,4-Dimethylbenzene	106
11	Styrene + 1,2-Dimethylbenzene	104 + 106
12	2-Methyl-2-cyclopenten-1-one	96
13	Isopropylbenzene	120
14	Propenylbenzene	120
15	Propylbenzene	120
16	1-Methyl-3-ethylbenzene	120
17	1-Methy-4-ethylbenzene	120
18	1,3,5-Trimethylbenzene	120
19	Methylstyrene + 1-Methyl-2-ethylbenzene	118 + 120
20	Methylstyrene	118
21	Indane	118
22	Methoxyphenol	108
23	Indene	116
24	C_4 Benzene	134
25	Acetophenone	120
26	C_4 Benzene	134
27	$C_{4:1}$ Benzene	132
28	Dimethoxybenzene (123, 138)	138
29	C_1 Indene	130
30	Naphthalene	128
31	Methylbenzoic acid methyl ester	150
32	C_2 Indene	144
33	Indanone	132
34	Methylnaphthalene	142
35	Methoxybenzoic acid methyl ester	166
36	Trimethoxybenzene	168
37	C_3 Indene	158
38	Diaromatic $C_{12}H_{10}$	154
39	Ethylnaphthalene	156
40	C_2 Naphthalene	156
41	$C_{2:1}$ Naphthalene	154
42	Acenaphthylene	152
43	Dibenzoic acid methyl ester	194
44	C_3 Naphthalene	170
45	Diaromatic	168
46	Dimethoxybenzoic acid methyl ester	196
47	Diaromatic $C_{13}H_{10}$ (e.g., Fluorene)	166
48	Triaromatic $C_{14}H_{10}$	178

* Peak numbers refer to Fig. 8. C_1 to C_4 (e.g. C_4 Benzene) indicate the number of carbon atoms attached.

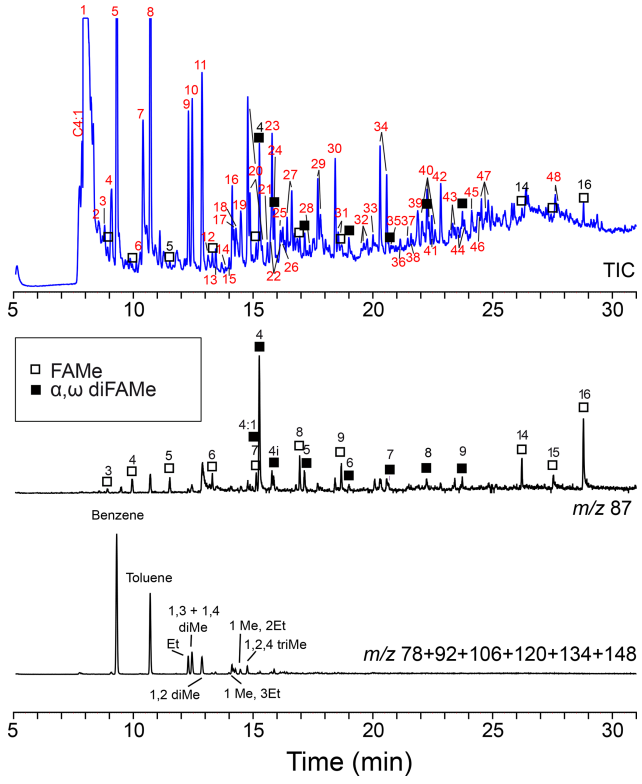

Figure 7. Chromatogram and mass chromatograms of *Thalassiphora pelagica* cysts from the Kerguelen Plateau after THM-GC-MS. Open squares are *n*-alkanoic acids; closed squares are *n*-alkanedioic acids. Black numbers indicate the number of carbon atoms of the compound. Red numbers refer to compound names listed in Table 2. **(a)** shows total ion current (TIC); **(b)** shows a mass chromatogram of $m/z = 87$ showing methyl esters of *n*-alkanoic acids and *n*-alkanedioic acids; 4 : 1 refers to the butenedioic acid, and 4i refers to the iso-butanedioic acid. FAMe stands for fatty acid methyl ester.

lassiphora produces cysts that belong to the degradation-resistant group, as is apparent from their morphology. This also explains their survival in the Kerguelen Plateau sediments.

The spectra of the *Thalassiphora* cysts from the Kerguelen Plateau are very similar to those of the culture-derived *Lingulodinium* cysts (Fig. 2a), except for the considerably lower absorptions for the E and F bands (various C-O stretching modes). This similarity implies only little change to the cyst macromolecule.

Since this is not accompanied by a loss in band A (O-H), we attribute this difference primarily to a relative loss in ether bonds rather than hydroxyl groups. In the Kerguelen Plateau setting the relative decrease in ether bonds is likely to be achieved through oxidation of the carbohydrate. This leads to ring-opening and chain-breaking and increases the relative abundance of carboxylic acids, aldehydes and ketones, which in turn may increase the intramolecular and intermolecular hydrogen bonding (Potthast et al., 2006) and thus reduce the relative abundance of ether bonds. Additionally, oxidative cross-linking may add carboxylic acids to the cyst wall, a process already starting before burial (Blom, 1936; Harvey et al., 1983; Stankiewicz et al., 2000; Versteegh et al., 2004). Plankton is rich in unsaturated fatty acids that will reach the seafloor and play a role in early diagenesis. Oxidative cross-linking primarily attacks the double bonds of unsaturated fatty acids, leading to fragmentation of the fatty acids and a cross-linking. This addition will increase in O-H and C = O relative to CH_2 (Lazzari and Chiantore, 1999; Scalarone et al., 2001). The carboxylic groups are less reactive and remain largely unaltered during this process (Scalarone et al., 2001). This condensation process thus also adds C = O, O-H, and CH_2 and reduces the relative proportion of ether bonds in the resulting cyst geomacromolecule.

The spectra of the *Thalassiphora* cysts from the Rhine Graben differ more from the spectra of culture-derived *Lingulodinium* cysts than the cysts from the Kerguelen Plateau (Fig. 2b). Compared to the latter, there is significantly less absorption in band A (O-H) and more in band B (CH_x) (Fig. 2c), whereas in band D the broad maximum at 1407 cm^{-1} splits giving rise to maxima at 1448 (CH_2 deformation and CH_3 asymmetric deformation) and 1376 cm^{-1} (CH_3 deformation). In contrast to cysts of *T. pelagica* from the Kerguelen plateau, the cysts from the Rhine Graben have been deposited in an environment with sulfidic conditions (Versteegh et al., 2007); the sedimentation rate and the sedimentary OM content are an order of magnitude higher (Pross and Schmiedl, 2002). In this sulfidic environment with ample labile OM the most clear explanation is the addition of longer-chain aliphatics, such as carboxylic acids, to the cyst wall through anaerobic cross-linking, such as natural vulcanization. Reactive sulfur species particularly attack aldehydes; ketones; and conjugated, distal and, to a lesser extent, mid-chain C = C double bonds but react much less with carboxyl and hydroxyl groups (Viaravamurthy and Mopper, 1987; Schouten et al., 1994a, b; Hebting et al., 2006). The strong decrease in O-H absorption and increase in C = O seem to disagree with this. However, the initial carbohydrate-based cyst wall is intrinsically poor in O-H and C = O, and chemical modification such as addition of alkanoic acids automatically decreases the relative abundance of these bond types and increases CH_x and C = O. Moreover, in this anaerobic environment oxygen as a powerful electron acceptor is in high demand and will selectively be removed, contributing to the loss of hydroxyl groups of the cyst macromolecule. Also here, the ample available polyunsaturated carboxylic acids from the marine plankton, including the dinoflagellate cysts of which many died without hatching (Pross, 2001), provide a rich source of lipids for this process, increasing the relative abundances of foremost CH_2 and C = O relative to C-O and O-H. Available clay minerals and free metal ions may have played a catalytic role (e.g., Schiffbauer et al., 2014), primarily outside the cyst wall.

As discussed above, both the Kerguelen Plateau and the Rhine Graben sedimentary environments have modified the *T. pelagica* cysts, albeit in different ways. Infra-red analysis of extant cysts of other members of this group of Gonyaulacoid dinoflagellate cysts show structural differences between the species (Versteegh et al., 2012; Bogus et al., 2014; Mertens et al., 2016; Gurdebeke et al., 2018; Luo et al., 2018). Hence, the question arises of which part of the differences recorded between the spectra of these *T. pelagica* with other Gonyaulacoid taxa arises from differences in cyst biosynthesis and what part arises from postmortem modification. The spectra of the recent Gonyaulacoid cysts show a consistent pattern in their order of absorption strength for bands D, E and F, with band F being strongest and band E weakest. This pattern is also seen for the cysts from the Kerguelen Plateau. However, for band C this is more complicated. Analysis of recent cysts by Bogus et al. (2014) shows for all members of the Gonyaulacaceae (*Lingulodinium, Spiniferites, Impagidinium, Protoceratium*) a band C with weaker absorption than bands D and E. In Gurdebeke et al. (2018), all members of the gonyaulacacean *Spiniferites* (except *S. pachydermus* the spectrum of which was taken from Bogus et al., 2014) show a strong absorption near $1600\,cm^{-1}$ in band C that exceeds the absorptions in band D. We also see this for *T. pelagica*, which when considering the variability of this band in recent cysts, we consider an intrinsic feature of the biopolymer. In band C, recent gonyaulacacean cysts also show a shoulder near $1705\,cm^{-1}$, which is always of less amplitude than the absorption $1590\,cm^{-1}$. This is clearly different for *T. pelagica* for which the absorption at $1705\,cm^{-1}$ is the most pronounced in band C, and for this difference with recent cysts we attribute the high absorption at $1705\,cm^{-1}$ for *T. pelagica* to diagenesis.

To get a better insight into the role of diagenesis, we have to directly compare the cysts from the Rhine Graben and the Kerguelen Plateau (Fig. 2c). They represent the same species: *T. pelagica*. Therefore, we may assume identical or at least closely similar chemical structures prior to diagenesis so that all spectral differences between them logically reflect differences in preservation. Clearly, this only provides the accumulated differences, and changes common to both the cysts from the Kerguelen Plateau and the Rhine Graben are not apparent. The differences lie foremost in the higher contribution of band A (O-H) and lower contribution of band B (CH_x) for the cysts from the Kerguelen plateau. The spectrum of these cysts from the Kerguelen Plateau also more closely matches the spectrum of *L. polyedrum*. Indeed, with the stronger absorption by CH_x and relatively weak absorptions of the other bands, the spectrum of the Rhine Graben specimens has become much more similar to that of the algaenan walls of green algae, such as *C. emersonii* (Fig. 2d; Allard, and Templier, 2001) or *Tetraedron minimum* (Blokker et al., 1998; Goth et al., 1988), albeit without the absorption at $718\,cm^{-1}$ and thus lacking the long carbon chains of algaenan.

As such, it appears on the basis of infrared spectroscopy of both *Thalassiphora* samples, in comparison to recent cysts from cultures and surface sediments, that we must assume that part of the observed differences with the *Lingulodinium* cysts may result from differences in cyst biosynthesis. The infrared spectra of recent *L. polyedrum* and fossil *T. pelagica* from the Kerguelen Plateau are very similar, suggesting that the cysts of *L. polyedrum* are a good modern analogue. Nevertheless, the stronger absorption for the fossil cysts of probably conjugated carbonyl at $1705\,cm^{-1}$ can be assigned to diagenesis. Further comparison with *Lingulodinium* shows that cysts from the Kerguelen Plateau are depleted in ether bonds. We attribute this depletion to modification of the cyst wall by oxidation and oxidative cross-linking. The cysts from the Rhine Graben differ considerably more from the *L. polyedrum* cysts than those from the Kerguelen Plateau. These differences are specifically an enrichment in CH_x and to a lesser extent C = O and show a relative loss of O-H. These differences are attributed to reactions by reactive sulfur species cross-linking the cyst wall and adding linear carbon chains to it. Furthermore, in the anaerobic depositional environment of the Rhine Graben, we expect cyst diagenesis to lead to a loss of oxygen, rather than an increase as we observe for the cysts from Kerguelen Plateau.

4.3 Py-GC-MS and THM-GC-MS

GC-MS results are consistent with the results of the infrared analyses, which suggest that differences in depositional environment are associated with differences in molecular structure. Pyrolysis of macromolecules consisting of long alkyl chains, such as algaenans or polyethylene, typically produces a series of alkane–alkene doublets (Fig. 5). The presence of such *n*-alkane–alkene doublets up to C_9 (and similarly C_7-C_{11} methyl-alkanone–alkenone doublets) in the cysts from the Kerguelen Plateau suggests that these have been derived from the cyst macromolecule. The length, up to C_9, may not be accidental since many unsaturated *n*-alkanoic acids have double bonds at ω-9 or closer to the end of the molecule, and oxidative cross-linking operates at such double bonds, whereby the remainder of the molecule may be released (e.g., Lazzari and Chiantone, 1999). Upon pyrolysis, the chains will break at these cross-links, resulting in a characteristic chain length distribution. The absence of alkane–alkene doublets from C_{10} in these cysts suggests that the aliphatic chains were relatively short, which agrees with the absence of an absorption near $720\,cm^{-1}$ in the infrared spectrum. The absence of $> C_{10}$ *n*-alkanoic acids supports this further. The presence of a minor abundance of *n*-alkanes without accompanying *n*-alkenes for C_{14}–C_{21} and their absence for C_{10}–C_{13} suggests that these C_{14}–C_{21} *n*-alkanes were either not covalently bound to the cyst macromolecule and may thus have been absorbed by the cyst wall and failed to be removed upon extraction or were exclusively ester-bound so that upon their release no *n*-alkenes were formed.

For the Kerguelen Plateau cysts, we find a similar gap in distribution in the *n*-alkanoic methyl-esters released upon and methylated by the thermochemolysis with C_{10}–C_{13} absent and C_{14}–C_{16} present but with no longer chains (Fig. 6). The absence of the ubiquitous C_{18} *n*-alkanoic methyl ester indicates that these longer C_{14}–C_{16} chains are not simply contamination but that these were also associated with the cysts themselves. In dinoflagellates, the saturated carboxylic acids are often dominated by C_{16} with C_{14} second in abundance (e.g., Robinson et al., 1987; Mansour et al., 1999; Mooney et a., 2007; Chu et al., 2009), and this same pattern obtained by thermochemolysis supports the hypothesis that these lipids originate from the nearest source, the dinoflagellate cytoplasm. The shorter C_3-C_9 *n*-alkenoic methyl esters are accompanied by (C_4-C_9) alkanedioic dimethyl esters with a strong dominance of the C_4 representative and provide evidence for a cyst wall with short-chain ester-cross-linked moieties. Fresh *L. polyedrum* cysts do not show any aliphatic signature, thus we attribute the aliphatic signature in the *T. pelagica* cyst wall to diagenetic modification of the initial macromolecule.

The thermochemolysis of cultured *L. polyedrum* cysts produced a series of mono- to penta-methoxy-benzenes, evidencing the carbohydrate hydroxy groups in the cyst-wall polymer (Versteegh et al., 2012). We observe tri-methoxy-benzenes as thermochemolysis products of the cysts from the Kerguelen Plateau, but they are of much lower abundance. This suggests that the carbohydrate nature is still recognizable in these fossil cysts. In contrast to this, di- to penta-methoxy-benzenes have not been detected as thermochemolysis products of the cysts from the Rhine Basin, indicating that for those cysts the carbohydrate nature has been entirely lost.

For the *T. pelagica* cysts from Kerguelen Plateau, the detection of benzenes with up to nine attached carbon atoms and phenols with up to four attached carbon atoms fully agrees with the observed chain length distribution of the aliphatic component and again suggests a macromolecule with carbon chains shorter than C_9. These series are longer than for the cultured *L. polyedrum* cysts but shorter than for the *T. pelagica* cysts from the Rhine Graben.

The stronger diagenetic alteration and sulfurization of the material from the Rhine Graben is also reflected by the relatively higher abundance of masses characteristic for sulfur (m/z 64, SO_2) and alkylthiophenes (m/z 97, 111, 125 and 139, together with a contribution by longer *n*-alkenes), whereas oxygen-containing moieties are more abundant in the material from the Kerguelen Plateau (m/z 93, 107, 121, 135 from phenols and m/z 95, 145 from benzofurans), as are alkylbenzenes (m/z 79, 105, 119, 133) (Fig. 8). Comparison to mass distributions of pyrolysates of other macromolecules (Fig. 6) demonstrates the much lower aliphatic contribution of the Kerguelen material and the disappearance of oxygen from and addition of sulfur to the cysts from the Rhine Graben.

4.4 Cyst wall diagenesis, diagenetic processes and implications

The diagenetic modification of the cyst walls is complex and involves different processes at different times and in different environments. We do not pretend that we can resolve all these processes and modifications. What we can identify is the presence of sulfurization, the presence of linear carbon chains and the extent to which the resulting cyst geomolecule deviates from the modern analogue biomolecule.

As a result of the very different sedimentary environments of the Rhine Graben and the Kerguelen Plateau, the initially identical cyst biomacromolecules of the *T. pelagica* cysts have been transformed into clearly different geomacromolecules. The cyst geomolecule from the Kerguelen Plateau still contains a lot of oxygen-bearing functionalities, and only a small amount of predominantly short linear carbon chains have been detected. Upon thermochemolysis, the carbohydrate nature of the wall material can still be evidenced. This is explained by the paleoenvironmental setting with oligotrophic surface waters, the aerobic depositional environment and low sedimentation rates. Here, oxic degradation and oxidative cross-linking prevail during transport of OM through the water column and in the surface sediments. We consider these processes to be the most important modifiers of the cyst macromolecule for the Kerguelen Plateau environment. In such an environment with considerable oxygen exposure times all but the most refractory OM has been rapidly remineralized aerobically, resulting in organic carbon lean sediments and only a little substrate to contribute to the cyst walls through oxidative cross-linking. In contrast to this, anoxia prevailed in the water column and sediment in the Rhine Graben environment. The Rhine Graben sediments remained rich in lipids and more refractory OM (Böcker et al., 2017) due to thermodynamic limitation of OM degradation under anaerobic (compared to aerobic) conditions (e.g., Arndt et al., 2013). As a result, there is ample substrate to react with the cyst biomacromolecule, which explains the ample presence of linear carbon chains (up to C_{20}) associated with the cyst wall. The presence of alkyl thiophenes in the pyrolysate identifies natural sulfurization as one of the mechanisms turning the cyst biomacromolecule into a geomacromolecule. As a result of the diagenetic modification, the cysts macromolecule shows an overall loss of oxygen-bearing functional groups and its carbohydrate signature can not be evidenced anymore upon thermochemolysis. On the basis of the results from pyrolysis, thermochemolysis and infrared analyses it appears that the cysts from the Kerguelen Plateau structurally more closely resemble the recent analogue than the cysts from the Rhine Graben and as such display better structural preservation. The cysts from the Rhine Graben not only display stronger intermolecular cross-linking, but structural changes to the initial molecule also resulted in loss of its the carbohydrate signature upon thermochemolysis.

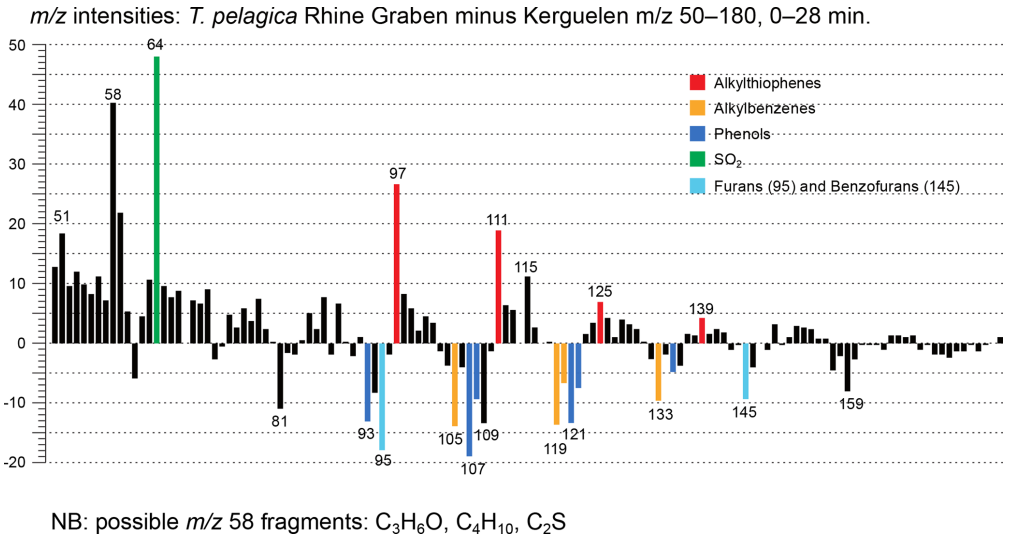

Figure 8. Relative mass intensities of the total chromatograms of *Thalassiphora pelagica* from the Rhine Graben minus those of *Thalassiphora pelagica* from the Kerguelen Plateau (Versteegh et al., 2007). Masses with abundances < 0 are more abundant in the specimens from the Kerguelen Plateau. Note the masses indicating sulfur-containing fragments (thiophenes) are more important in the specimens from the Rhine Graben, whereas masses characterizing oxygen-containing fragments (furans, phenols) and alkylbenzenes are more abundant in specimens from the Kerguelen Plateau.

Experiments show that both the oxidative cross-linking (Lazzari and Chiantore, 1999; Scalarone et al., 2001) and sulfurization (Schouten et al., 1994a, b) preferably attack double bonds. Subsequently, the activated group cross-links with a nearby carbon atom or functional group of the same (macro)molecule or a different one. For oxidative cross-linking the aliphatic chain may break at the double bond position during this process, which could provide an additional explanation for the absence of long carbon chains in the pyrolysate of the cysts from the Kerguelen Plateau. As far as we are aware, this shortening mechanism has not been observed for natural sulfurization. Furthermore, and not surprisingly, the aerobically modified cysts appear to be rich in oxygen-bearing functionalities, whereas a general loss of such functionalities is observed for the cysts from the anaerobic setting. This difference in organically bound oxygen provokes the speculation that repeatedly changing OM from oxic to anoxic states such as what occurs in bioturbated sediments effectively supplies the anoxic environment with organically bound oxygen, facilitating anaerobic OM degradation, whereas the change from anoxic to oxic conditions enables aerobic processes to oxidize labile functionalities created anaerobically. This could be an additional explanation as to why redox oscillation promotes OM remineralization (Aller, 2001).

For the Kerguelen Plateau, the aerobic degradation will rapidly decrease the OM concentration, foremost for the most reactive and labile components. As such, the rate of modification of the cyst molecular structure as a result of interaction with other OM will rapidly decrease. Due to ongoing sedimentation, the cysts will get out of the reach of oxygen diffusing into the sediment and enter the suboxic zone. The low concentration and refractory nature of the remaining OM will have allowed for low suboxic diagenetic rates too, and the system will have never reached the sulfate reduction zone. Therefore, we consider that for the cysts from the Kerguelen Plateau, by far most molecular change will have been in an early, aerobic stage, especially with respect to interaction with other OM.

In contrast to this, the Rhine Graben sediments have an order of magnitude higher OM contents, whereas the anaerobic redox environment promotes the production and accumulation of small, relatively labile organic molecules and reactive sulfur species. Initially, with a lot of fresh OM, mineralization rates were similar to aerobic environments (Arndt et al., 2013). We suggest that this also accounts for the diagenetic modification of the cyst molecule. In contrast to the Kerguelen Plateau, the high OM content must have supported active anaerobic degradation and with it the generation of reactive organic and inorganic molecules for a much longer time. Therefore, it seems logical that the accumulated molecular change (through intermolecular cross-linking and structural modification) of the cysts from the Rhine Graben is larger than for the cysts from the Kerguelen Plateau.

Finally, despite the changes taking place to the *T. pelagica* cysts at a molecular level, at a microscopic level nothing from these changes is apparent. Therefore, excellent morphologic preservation is no proof of excellent molecular preservation, and this should be kept in mind, e.g., upon isotopic analyses of OM. Fortunately, a simple infrared analysis, at least in our example, may be sufficient to identify to what extent chemical modification may have taken place. Finally, the nature of

the cysts is such that they belong intrinsically to the refractory OM so that the changes brought about in the anaerobic environment do not introduce bias due to a higher presence of these cysts in the fossil record.

5 Conclusions

By analyzing remains of the same species (*T. pelagica*) from two contrasting environmental settings, differences in the composition of the starting material can be excluded. As such, all chemical differences between the cysts from the different depositional settings can be assigned to postmortem modification of the original biomacromolecule. However, alteration processes that the different settings have in common will remain undetected and requires knowledge of the initial state. Here we circumvent the absence of such material by comparing to a close analogue, recent cysts of *L. polyedrum.*

Analysis of the composition and structure of *T. pelagica* cysts from the Kerguelen Plateau and comparison to recent cysts of gonyaulacoid dinoflagellates, the group of which *Thalassiphora* is a member, shows that the fossil cysts to a large extent have been structurally preserved. Diagenetic modification is mainly confined to an increase in C = O, a loss of C-O and presumably an increase in hydrogen bridges. Thermochemolysis generates di- and tri-methoxybenzenes despite a strong decrease in their production, indicating that part of the carbohydrate's nature is preserved. The presence of carbon chains up to C_{11} is also attributed to diagenesis since such an aliphatic component is absent in culture-derived gonyaulacoid cysts.

Comparison with modern gonyaulacoid cyst walls demonstrates that the *T. pelagica* cysts from the Kerguelen Plateau and Rhine Graben have been structurally changed by diagenetic intermolecular cross-linking and by intermolecular modification. Both processes were stronger for cysts from the Rhine Graben than the 10 Ma younger specimens of the same species from the Kerguelen Plateau, despite the absence of any visual indication for these differences upon microscopic examination. In contrast to the cysts from the Kerguelen Plateau, the cysts from the Rhine Graben lost their carbohydrate signature of the initial biomacromolecule. We attribute this to a stronger diagenetic change enforced by the organic rich and sulfidic diagenetic setting the Rhine Graben material has been subject to. This study demonstrates the advantage of using organic particles of narrowly defined (species-level) biological sources for unraveling postmortem modification of OM. It also shows that excellent morphological preservation does not imply excellent structural preservation at molecular level and that the postmortem modification of the same initial biomacromolecule can differ considerably between sedimentary settings. Furthermore, it leads to the counterintuitive conclusion that the best preservation of molecular structure may not be found where most OM is preserved.

Data availability. Data are available at: https://doi.pangaea.de/10.1594/PANGAEA.905696 (last access: 8 June 2020, Versteegh et al., 2019).

Supplement. The supplement related to this article is available online at: https://doi.org/10.5194/bg-17-3545-2020-supplement.

Author contributions. GJMV collected the geochemical data interpreted them and wrote the manuscript. AJPH provided the material and did the palynology. KAFZ was responsible for project funding and administration and together with GJMV formulated the overarching research goals and aims. All authors discussed data and earlier versions of the manuscript.

Competing interests. The authors declare that they have no conflict of interest.

Acknowledgements. We thank Henk Brinkhuis (Utrecht University, Royal NIOZ) for his constructive comments on the manuscript. We also thank the reviewers for their constructive comments, which significantly improved the manuscript. IODP is thanked for providing the sample utilized in this study.

Financial support. This research has been supported by the Deutsche Forschungsgemeinschaft (grant no. MER/MET 17-87).

The article processing charges for this open-access publication were covered by the University of Bremen.

Review statement. This paper was edited by Silvio Pantoja and reviewed by Morgan Raven and Jakob Vinther.

References

Allard, B. and Templier, J.: Comparison of neutral lipid profile of various trilaminar outer cell wall (TLS)-containing microalgae with emphasis on algaenan occurrence, Phytochem., 54, 369–380, https://doi.org/10.1016/S0031-9422(00)00135-7, 2000.

Allard, B. and Templier, J.: High molecular weight lipids from the trilaminar outer wall (TLS)-containing microalgae *Chlorella emersonii, Scenedesmus communis* and *Tetraedron minimum*, Phytochem., 57, 459–467, https://doi.org/10.1016/S0031-9422(01)00071-1, 2001.

Aller, R. C.: Transport and reactions in the bioirrigated zone, in: The Benthic Boundary Layer, edited by: Boudreau, B. P. and Jørgensen, B. B., Oxford University Press, Oxford, 269–301, 2001.

Arndt, S., Jørgensen, B. B., LaRowe, D. E., Middelburg, J. J., Pancost, R. D., and Regnier, R.: Quantifying the degradation of organic matter in marine sediments: A review and synthesis, Earth-Sci. Rev. 123, 53–86, https://doi.org/10.1016/j.earscirev.2013.02.008, 2013.

Bianchi, T. S., Schreiner, K. M., Smith, R. W., Burdige, D. J., Woodart, S., and Conley, D. J.: Redox Effects on Organic Matter Storage in Coastal Sediments During the Holocene: A Biomarker/Proxy Perspective, Ann. Rev. Earth Planet. Sci., 44, 295–319, https://doi.org/10.1146/annurev-earth-060614-105417, 2016.

Blokker, P., Schouten, S., van den Ende, H., de Leeuw, J. W., Hatcher, P. G., and Sinninghe Damsté, J. S.: Chemical structure of algaenans from the fresh water algae *Tetraedron minimum, Scenedesmus communis* and *Pediastrum boryanum*, Org. Geochem., 29, 1453–1468, https://doi.org/10.1016/S0146-6380(98)00111-9, 1998.

Blom, A. V.: Quelques remarques sur le mécanisme de séchage des peintures à l'huile, Peintures, Pigments, Vernis, 13, 156–162, 1936.

Bogus, K., Harding, I. C., King, A., Charles, A. A., Zonneveld, K. A. F., and Versteegh, G. J. M.: The composition and diversity of dinosporin in species of the *Apectodinium* complex (Dinoflagellata), Rev. Palaeobot. Palynol., 183, 21–31, https://doi.org/10.1016/j.revpalbo.2012.07.001, 2012.

Bogus, K., Mertens, K. N., Lauwaert, J., Harding, I. C., Vrielinck, H., Zonneveld, K. A. F., and Versteegh, G. J. M.: Differences in the chemical composition of organic-walled dinoflagellate resting cysts from phototrophic and heterotrophic dinoflagellates, J. Phycol., 50, 254–266, https://doi.org/10.1111/jpy.12170, 2014.

Böcker, J., Littke, R., and Forster, A.: An overview on source rocks and the petroleum system of the central Upper Rhine Graben. Int J Earth Sci (Geol Rundsch) International Journal of Earth Sciences: GR Geol. Rundschau 106, 707–742, https://doi.org/10.1007/s00531-016-1330-3,2017.

Butterfield, N. J.: Organic preservation of non-mineralizing organisms and the taphonomy of the Burgess Shale, Paleobiol., 16, 272–286, https://doi.org/10.1017/S0094837300009994, 1990.

Colthup, N. B., Daly, L. H., and Wiberly, S. E.: Introduction to Infrared and Raman Spectroscopy, Academic Press Limited, London, 547 pp., 1990.

Chu, F.-L. E., Lund, D., Littreal, R., Ruck, E., and Harvey, E.: Species-specific differences in long-chain n-3 essential fatty acid, sterol, and steroidal ketone production in six heterotrophic protist species, Aquat. Biol. 6, 159–172, https://doi.org/10.3354/ab00174, 2009.

de Leeuw, J. W. and Largeau, C.: A review of macromolecular compounds that comprise living organisms and their role in kerogen, coal and petroleum formation, edited by: Engel M. H. and Macko S. A., in: Organic Geochemistry, Principles and Applications, Plenum Press, New York, 23–72, https://doi.org/10.1007/978-1-4615-2890-6_2, 1993.

de Leeuw, J. W., Versteegh, G. J. M., and van Bergen, P. F.: Biomacromolecules of plants and algae and their fossil analogues, Plant Ecol., 189, 209–233, https://doi.org/10.1007/s11258-005-9027-x, 2006.

Durand, B.: Sedimentary organic matter and kerogen, Definition and quantitative importance of kerogen, edited by: Durand, B., in: Kerogen: Insoluble Organic Matter from Sedimentary Rocks, Editions Technip, Paris, 13–34, 1980.

Ellegaard, M., Figueroa, R., and Versteegh, G. J. M.: Dinoflagellate life cycles and diversity: key foci for future research, edited by: Lewis J. M., Marret F., and Bradley L., in: Biological and Geological Perspectives of Dinoflagellates, Geol. Soc. London, 241–254, https://doi.org/10.1144/TMS5.24, 2013.

Gatellier, J. P. L. A., de Leeuw, J. W., Sinninghe Damsté, J. S., Derenne, S., Largeau, C., Metzger, P.: A comparative study of macromolecular substances of a Coorongite and cell walls of the extant alga *Botryococcus braunii*, Geochim. Cosmochim. Ac., 57, 2053–2068, https://doi.org/10.1016/0016-7037(93)90093-C, 1993.

Goth, K., de Leeuw, J. W., Püttmann, W., and Tegelaar, E. W.: Origin of Messel Oil Shale kerogen, Nature, 336, 759–761, https://doi.org/10.1038/336759a0, 1988.

Gupta, N. S., Briggs, D. E. G., Collinson, M. E., Evershed, R. P., Michels, R., and Pancost, R. D.: Molecular preservation of plant and insect cuticles from the Oligocene Enspel Formation, Germany: Evidence against derivation of aliphatic polymer from sediment, Org. Geochem., 38, 404–418, https://doi.org/10.1016/j.orggeochem.2006.06.012, 2007.

Gurdebeke, P. R., Mertens, K. N., Bogus, K., Marret, F., Chomérat, N., Vrielinck, H., Louwye, S.: Taxonomic re-investigation and geochemical characterization of Reid's (1974) species of Spiniferites from holotype and topotype material, Palynol., https://doi.org/10.1080/01916122.2018.1465735, 2018.

Harvey, G. R., Boran, D. A., Chesal, L. A., and Tokar, J. M.: The structure of marine fulvic and humic acid, Mar. Chem., 12, 119–132, https://doi.org/10.1016/0304-4203(83)90075-0, 1983.

Hebting, Y., Schaeffer, P., Behrens, A., Adam, P., Schmitt, G., Schneckenburger, P., Bernasconi, S. M., and Albrecht, P.: Biomarker evidence for a major preservation pathway of sedimentary organic carbon, Science, 312, 1627–1631, https://doi.org/10.1126/science.1126372, 2006.

Hedges, J. I. and Keil, R. G.: Sedimentary organic matter preservation: an assessment and speculative synthesis, Mar. Chem. 49, 81–115, https://doi.org/10.1016/0304-4203(95)00008-F, 1995.

Herman, B. M.: Infra-red absorption, scattering, and total attenuation cross-sections for water spheres, Q. J. Roy. Meteor. Soc., 88, 143–150, 1962.

Hoefs, M. J. L., Rijpstra, W. I. C., and Sinninghe Damsté, J. S.: The influence of oxic degradation on the sedimentary biomarker record I: Evidence from Madeira Abyssal Plain turbidites, Geochim. Cosmochim. Ac., 66, 2719–2735, https://doi.org/10.1016/S0016-7037(02)00864-52 2002.

Kohnen, M. E. L., Sinninghe Damsté, J. S., ten Haven, H. L., and de Leeuw, J. W.: Early incorporation of polysulfides in sedimentary organic matter, Nature, 341, 640–641, https://doi.org/10.1038/341640a0, 1989.

Kutuzov, I., Rosenberg, Y. O., Bishop, A., and Amrani, A.: The Origin of Organic Sulphur Compounds and Their Impact on the Paleoenvironmental Record, edited by: Wilkes H., in: Hydrocarbons, Oils and Lipids: Diversity, Origin, Chemistry and Fate, Springer, https://doi.org/10.1007/978-3-319-54529-5_1-1, 2019.

Lazzari, M. and Chiantore, O.: Drying and oxidative degradation of linseed oil, Polymer Degr. Stabil. 65, 303–313, https://doi.org/10.1016/S0141-3910(99)00020-8, 1999.

Lin, R. and Ritz, G. P.: Reflectance FT-IR microspectroscopy of fossil algae contained in organic-rich shales, Appl. Spectroscopy, 47, 265–271, https://doi.org/10.1366/0003702934066794, 1993.

Luo, Z., Lim, Z. F., Mertens, K. N., Gurdebeke, P., Bogus, K., Carbonell-Moore, M. C., Vrielinck, H., Leaw, C. P., Lim, P. T., Chomérat, N., Li, X., and Gu, H.: Morpho-molecular di-

versity and phylogeny of *Bysmatrum* (Dinophyceae) from the South China Sea and France, European, J. Phycol., 53, 318–335, https://doi.org/10.1080/09670262.2018.1449014, 2018.

Mansour, M. P., Volkman, J. K., Jackson, A. E., and Blackburn, S. I.: The fatty acid and sterol composition of five marine dinoflagellates, J. Phycol., 35, 710–720, https://doi.org/10.1046/j.1529-8817.1999.3540710.x, 1999.

McMurry, H. L. and Thornton, V.: Correlation of Infrared Spectra, Anal. Chem., 24, 318–334, https://doi.org/10.1021/ac60062a018, 1952.

Mertens, K. N., Gu, H., Takano, Y., Price, A. M., Pospelova, V., Bogus, K., Versteegh, G. J. M., Marret, F., Turner, R. E., Rabalais, N. N., and Matsuoka, K.: The cyst-theca relation of *Trinovantedinium pallidifulvum*, with erection of *Protoperidinium lousianensis* sp. nov. and their phylogenetic position within the *Conica* group, Palynol., 41, 183–202, https://doi.org/10.1080/01916122.2016.1147219, 2016.

Mooney, B. D., Nichols, P. D., de Salas, M. F., and Hallegraeff, G. M.: Lipid, fatty acid and sterol composition of eight species of Kareniaceae (Dinophyta): chemotaxonomy and putative lipid phycotoxins, J. Phycol., 43, 101–111, https://doi.org/10.1111/j.1529-8817.2006.00312, 2007.

Nierop, K. G., Reichart, G., Veld, H., and Sinninghe Damsté, J. S.: The influence of oxygen exposure time on the composition of macromolecular organic matter as revealed by surface sediments on the Murray Ridge (Arabian Sea), Geochim. Cosmochim. Ac., 206, 40–56, https://doi.org/10.1016/j.gca.2017.02.032, 2017.

Nissenbaum, A. and Kaplan, I. R.: Chemical and isotopic evidence for the in situ origin of marine humic substances, Limnol. Oceanogr., 17, 570–582, https://doi.org/10.4319/lo.1972.17.4.0570, 1972.

Nunn, S. and Nishikida, K.: Advanced ATR correction algorithm, Thermo Fisher Appl. Notes., Note 50581, 1–3, 2008.

Robinson, N., Cranwell, P. A., Eglinton, G., and Jaworski, G. H. M.: Lipids of four species of freshwater dinoflagellates, Phytochemistry, 26, 411–421, https://doi.org/10.1016/S0031-9422(00)81423-5, 1987.

Potthast, A., Rosenau, T., and Kosma, P.: Analysis of Oxidized Functionalities in Cellulose, Adv. Polym. Sci., 205, 1–48, https://doi.org/10.1007/12_099, 2006.

Rontani, J. F.: Photooxidative and autoxidative degradation of lipid components during the senescence of phototrophic organisms, in: Phytochemistry Research Progress, Nova Science Publishers, Hauppauge, NY, 115–144, 2008.

Pross, J.: Paleo-oxygenation in Tertiary epeiric seas: evidence from dinoflagellate cysts, Palaeogeogr. Palaeocl., 166, 369–381, https://doi.org/10.1016/S0031-0182(00)00219-4, 2001.

Pross, J. and Schmiedl, G.: Early Oligocene dinoflagellate cysts from the Upper Rhine Graben (SW Germany): paleoenvironmental and paleoclimatic implications, Mar. Micropaleontol., 45, 1–24, https://doi.org/10.1016/S0377-8398(01)00046-9, 2002.

Scalarone, D., Lazzari, M., and Chiantore, O.: Thermally assisted hydrolysis and methylation-pyrolysis-gas chromatography/mass spectrometry of light-aged linseed oil, J. Anal. Appl. Pyrol., 58, 503–512, https://doi.org/10.1016/S0165-2370(00)00127-3, 2001.

Schiffbauer, J. D., Xiao, S., Cai, Y., Wallace, A. F., Hua, H., Hunter, J., Xu, H., Peng, Y., and Kaufman, A. J.: A unifying model for Neoproterozoic–Palaeozoic exceptional fossil preservation through pyritization and carbonaceous compression, Nat. Commun., 5, 1–12, https://doi.org/10.1038/ncomms6754, 2014

Schouten, S., de Graaf, W., Sinninghe Damsté, J. S., Van Driel, G. B., and de Leeuw, J. W.: Laboratory simulation of natural sulfurization, 2. Reaction of multi-functionalized lipids with inorganic polysulfides at low-temperatures, Org. Geochem., 22, 825–834, https://doi.org/10.1016/0146-6380(94)90142-2, 1994a.

Schouten, S., van Driel, G., Sinninghe Damsté, J. S., and de Leeuw, J. W.: Natural sulphurisation of ketones and aldehydes: a key reaction in the formation of organic sulphur compounds, Geochim. Cosmochim. Ac., 58, 5111–5116, https://doi.org/10.1016/j.orggeochem.2007.06.007, 1994b.

Schlich, R. and Wise, S. W.: and Shipboard Scientific Party: Site 748, Proc. ODP Init. Repts. 120, College station, TX, 157–235, https://doi.org/10.2973/odp.proc.ir.120.110.1989, 1989

Stankiewicz, B. A., Briggs, D. E. G., Michels, R., Collinson, M. E., Flannery, M. B., and Evershed, R. P.: Alternative origin of aliphatic polymer kerogen, Geol., 28, 559–562, https://doi.org/10.1130/0091-7613(2000)28<559:AOOAPI>2.0.CO;2, 2000.

Stankiewicz, B. A., Scott, A. C., Collinson, M. E., Finch, P., Mösle, B., Briggs, D. E. G., and Evershed, R. P.: Molecular taphonomy of arthropod and plant cuticles from the Carboniferous of North America: implications for the origin of kerogen, J. Geol. Soc., 155, 453–462, https://doi.org/10.1144/gsjgs.155.3.0453, 1998.

Vandenbroucke, M. and Largeau, C.: Kerogen origin, evolution and structure, Org. Geochem., 38, 719–833, https://doi.org/10.1016/j.orggeochem.2007.01.001, 2007.

Versteegh, G. J. M., Blokker, P., Bogus, K., Harding, I., Lewis, J., Oltmanns, S., Rochon, A., and Zonneveld, K. A. F.: Infra red spectroscopy, flash pyrolysis, thermally assisted hydrolysis and methylation (THM) in the presence of tetramethylammonium hydroxide (TMAH) of cultured and sediment-derived *Lingulodinium polyedrum* (Dinoflagellata) cyst walls, Org. Geochem., 43, 92–102, https://doi.org/10.1016/j.orggeochem.2011.10.007, 2012.

Versteegh, G. J. M., Blokker, P., Wood, G., Collinson, M. E., Sinninghe Damsté, J. S., and de Leeuw, J. W.: An example of oxidative polymerization of unsaturated fatty acids as a preservation pathway for microalgal organic matter, Org. Geochem., 35, 1129–1139, https://doi.org/10.1016/j.orggeochem.2004.06.012, 2004.

Versteegh, G. J. M., Blokker, P., Marshall, C. R., and Pross, J.: Macromolecular composition of the dinoflagellate cyst *Thalassiphora pelagica* (Oligocene, SW Germany), Org. Geochem., 38, 1643–1656, https://doi.org/10.1016/j.orggeochem.2007.06.007, 2007.

Versteegh, G. J. M., Zonneveld, K. A. F., and de Lange, G. J.: Selective aerobic and anaerobic degradation of lipids and palynomorphs in the Eastern Mediterranean since the onset of sapropel S1 deposition, Mar. Geol., 278, 177–192, https://doi.org/10.1016/j.margeo.2010.10.00, 2010.

Versteegh, G. J. M., Houben, A. J. P., and Zonneveld, K. A. F.: Micro-FTIR and py-GC-MS data on Thalassiphora pelagica of ODP sample 120-748B-18H-17W,55-57, Pangaea Data Depository, available at: https://doi.pangaea.de/10.1594/PANGAEA.905696 (last access: 8 June 2020), 2019.

Wojdyr, M.: Fityk: a general-purpose peak fitting program, J. Appl. Crystallogr., 43, 1126–1128, https://doi.org/10.1107/S0021889810030499, 2010.

Vairavamurthy, A. and Mopper, K.: Geochemical formation of organosulphur compounds (thiols) by addition of H_2S to sedimentary organic matter, Nature, 329, 623–625, https://doi.org/10.1038/329623a0, 1987.

Zonneveld, K. A. F., Versteegh, G. J. M., Kasten, S., Eglinton, T. I., Emeis, K.-C., Huguet, C., Koch, B. P., de Lange, G. J., de Leeuw, J. W., Middelburg, J. J., Mollenhauer, G., Prahl, F. G., Rethemeyer, J., and Wakeham, S. G.: Selective preservation of organic matter in marine environments; processes and impact on the sedimentary record, Biogeosciences, 7, 483–511, https://doi.org/10.5194/bg-7-483-2010, 2010.

Zonneveld, K. A. F., Gray, D. D., Kuhn, G., and Versteegh, G. J. M.: Postdepositional aerobic and anaerobic particulate organic matter degradation succession reflected by dinoflagellate cysts: The Madeira Abyssal Plain revisited, Mar. Geol., 408, 87–109, https://doi.org/10.1016/j.margeo.2018.11.010, 2019.